Progress In Electromagnetics Research B, Vol. 56, 203–218, 2013

A HYBRID NUMERICAL-ANALYTICAL MODEL FOR THE ELECTROMAGNETIC CHARACTERIZATION OF THE ADMITTANCE MATRIX OF SCATTERING OBJECTS

Paola Russo[1, *], Desar Shahu[1], Alfredo De Leo[1], Valter Mariani Primiani[1], Lorenzo Scalise[2], and Graziano Cerri[1]

[1]Dipartimento di Ingegneria dell'Informazione, Università Politecnica delle Marche, Ancona, Italy

[2]Dipartimento di Ingegneria Industriale e Scienze Matematiche, Università Politecnica delle Marche, Ancona, Italy

Abstract—The aim of this work is to implement a hybrid approach able to provide an efficient solution of the electromagnetic coupling between an antenna and an obstacle distant few meters away. The idea is to divide the problem into a small number of less complex sub-problems exploiting the advantage of generating the admittance matrix that describes the scattering problem by a numerical code. To this end, the electromagnetic field impinging on the object has been characterized by means of a proper number of very narrow beams; for each beam the scattering problem has been solved by a commercial code; finally, the total admittance matrix has been obtained as composition of all the scattering contributions. The resulting echo of a moving obstacle has been compared with that measured by experimental investigations, both for metallic and dielectric bodies.

1. INTRODUCTION

The electromagnetic (EM) scattering from metallic or dielectric objects is addressed very frequently in the literature. Many numerical techniques have been developed, and they are mainly based on integral equations, as Method of Moments (MoM) [1] and the Discrete Dipole Approximation [2], or on the finite difference algorithm both in

Received 9 August 2013, Accepted 30 October 2013, Scheduled 1 November 2013

* Corresponding author: Paola Russo (paola.russo@univpm.it).

frequency domain, as the Finite Element Method [3], and in time domain, as the Finite Difference Time Domain (FDTD) [4–7].

Each of these techniques has certain advantages and some disadvantages. For example, the MoM is an extremely powerful technique, but requires the inversion of very large matrices or, the implementation of complex algorithms not always applicable to an irregular geometry [8]. In literature many papers proposed different algorithms for its application to dielectric, and non homogenous bodies, such as multilayer structures [9, 10] or composite metallic and dielectric structures [11].

When the reflecting object is geometrically complex, and non homogenous, the use of the MoM may require a strong computational effort.

On the other hand, the FDTD technique is also a very powerful tool, and in case of non-homogeneous, and geometrically complex objects is often preferred to the MoM. Its limit is given by the discretization of the whole computational domain, including the space that separates the antenna from the object. In this way, the demand for computational resources can be extremely costly, especially when dimensions are large compared to wavelength.

Many studies in the literature have dealt with the possibility of interfacing the two techniques to exploit their capabilities. For example in [12] a linear antenna is used to radiate a dielectric object. The MoM technique, applied in time domain, is used to simulate the antenna, while the FDTD technique is applied for simulating the dielectric object. The interaction between the two techniques is done using the principle of equivalence. In [13] a similar hybrid technique was presented, but the MoM is developed in frequency domain (MoM).

The MoM-FDTD hybrid technique is very powerful because allows the simulation of both situations in which the object is in the near field of the antenna as well as those where it is in the far field. Its limitation is mainly related to the application of the MoM to complex antenna geometry, and, when used in time domain, to the instabilities problem of the MoM. In addition, for parametric analysis, it is necessary to repeat every time the entire simulation and this aspect leads us to formulate a different hybrid approach to scattering problem.

In this paper a new technique for the solution of scattering problems is presented. The model is based on a generalized matrix approach, typical of the circuit theory, that leads to a formulation where the terms representing the scattering object and the terms regarding the impinging field are separated, and no matrix inversion is required. In this way a tool, very flexible and simple to implement, is developed, suitable for parametric analysis: for example it allows

studying the effects of changes concerning the antenna (type, distance from the scattering body, etc.) modifying only the corresponding terms, without repeating the whole procedure. The most significant aspect is the calculation of the admittance matrix of the scattering body, that is the matrix that relates the current distribution induced in the body with the incident field. The idea of this technique arises from the MoM, that evaluates the admittance matrix of the scattering object, inverting the impedance matrix of the moments. Once the admittance matrix of the object is known, it is possible to calculate the signal scattered under different conditions of exposure.

It is useful to mention the motivation that led us to develop this technique. In a previous work [14] we investigated the feasibility of a system for remote monitoring of human breathing activity. As a consequence of the feasibility study and from the analysis of the literature emerged the need to have an accurate model for the design of the electromagnetic system. Hence the need of a tool able to carry out an accurate and fast parametric analysis of the monitoring system performances, as for example the effect of the mutual position of the antenna and the body, the optimal distance between the antenna and the body, the minimum required sensitivity of the receiver, or the antenna characteristics.

The calculation of the admittance matrix is done with a direct method, and therefore no inversion of large matrices is required. The developed technique is hybrid because it combines some features of a numerical tool with the theory of microwave junctions.

The numerical technique used in this work is based on the Finite Integral Technique (FIT), and in particular, a commercial software (CST) was used [15], however the model is not limited to the type of numerical technique adopted. This choice was done because nowadays commercial software are able to handle complex geometries with small details. But if the investigation of problems where the EM interaction between source and scattering objects occurs in the far field region, the simulated box for a full-wave numerical solution may be so large to require the use of powerful computer clusters. In particular the proposed hybrid tool is able to both take the advantages of a commercial code and, at the same time, to reduce the whole problem into a sequence of small problems simpler to study and faster to solve.

The model is applied to a simple geometry in order to assess its accuracy and efficiency and to permit its validation also with measurements, both in the case of a metallic scattering object and for a penetrable body. The model is however quite general and may also be used with more complex geometries.

2. MODEL DESCRIPTION

The geometry of the problem is shown in Fig. 1. The target has mainly a 2-dimensional extension and exhibits a simple geometry in order to develop a first stage model and to verify its results with measurements in a repeatable scenario.

In a typical real situation the target is considered in the far field zone of the radiating antenna. When the incident field impinges on the target it creates a density current distribution that irradiates the scattered field detected by the antenna. The assumption of negligible influence of the scattered field on the antenna characteristics is adopted.

If the target surface facing the antenna is subdivided in N sub-areas (see Fig. 2) whose dimensions are chosen in order to consider

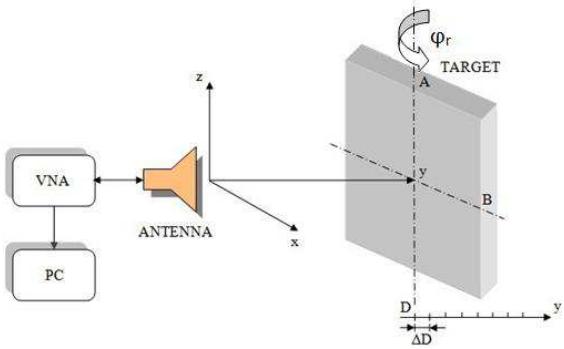

Figure 1. Simple block diagram of the system.

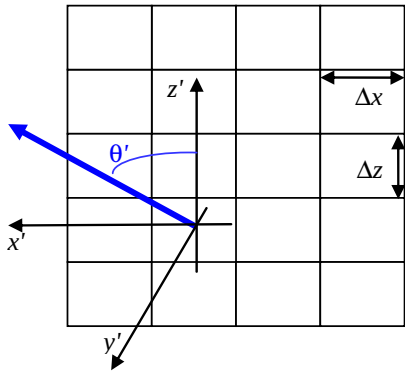

Figure 2. Discretized target.

the induced current distribution uniform on each sub-area, the current elements can be related to the incident field through an admittance matrix:

$$\begin{bmatrix} J_x \\ J_z \end{bmatrix}_{2Nx1} = \begin{bmatrix} Y_{xx} & Y_{xz} \\ Y_{zx} & Y_{zz} \end{bmatrix}_{2Nx2N} \cdot \begin{bmatrix} E_{inc\,x} \\ E_{inc\,z} \end{bmatrix}_{2Nx1} \tag{1}$$

where $[E_{inc\,s}]$ $(s = x, z)$ is the vector of the s-directed incident field on each sub-area of the target surface, $[J_s]$ the vector of the s-directed current density induced on each cell, and Y a matrix that depends on the geometry and material of the target, and on the frequency. The field component normal to the body surface is neglected because the incident field whose components are essentially tangent to the body, induces currents in the same directions. However this assumption is not a limitation for the type of exposure that can be handle by the method, in fact it also holds generally for lossy penetrable objects when the penetration depth is small enough so as only the currents flowing on a superficial layer generate the scattered field, as in the case of our example.

The assumption of uniform current in the cells allows to calculate analytically the reflected field after summing the contributions from each sub-area. From the vector potential, using the classical approach [16], the far field due to the uniform current flowing on p-th rectangular sub-area can be calculated:

$$\begin{aligned} \vec{E}_p^{\,s}(r,\theta',\phi') = -j\omega\vec{A}_p = -jk\eta\Delta x\Delta z\frac{e^{-jkr}}{4\pi r}\Big[\Big(\vec{J}_p\cdot\hat{x}\cos\theta\cos\phi - \vec{J}_p\cdot\hat{z}\sin\theta\Big)\hat{\theta} \\ -\Big(\vec{J}_p\cdot\hat{x}\sin\phi\Big)\hat{\phi}\Big]\frac{\sin(X')}{X'}\frac{\sin(Z')}{Z'} \end{aligned} \tag{2}$$

where J_p is the current in the p-th cell, whose amplitude and phase depends on the incident field according to Equation (1), $X' = \frac{k\Delta x}{2}\sin(\theta')\cos(\phi')$; $Z' = \frac{k\Delta z}{2}\cos(\theta')$, k is the wave number.

Equation (1) can be also seen as the typical representation of the solution of a scattering problem obtained for example with the Method of Moments after the inversion of an impedance matrix, set-up through the use of proper boundary conditions or constitutive relationships. In our case, we propose a method to evaluate directly the admittance matrix $[Y]$ without the necessity of the matrix inversion, using in particular the capabilities of a commercial code (CST Microwave Studio, in the present case), able to handle inhomogeneous and complex structures. The basic idea is inferred by the classic representation of circuits relationships with the admittance matrix.

By definition

$$Y_{xs,xt}^{m,n} = \left.\frac{J_{n,xs}}{E_{inc\,m,xt}}\right|_{E_{inc\,i}=0} \quad \text{for } i = 1,\ldots,N; \quad i \neq m \tag{3}$$

where $xs = (x, z)$, and $xt = (x, z)$.

The matrix element calculation according to Equation (3) requires that the incident field, polarized in the specified direction xt, illuminates the m-th sub-area only, whereas the remaining part of the target is not radiated. This is similar to consider the target as a multiport circuit, each port corresponding to a sub-area. To recover the (m, n) matrix element we have to feed the m-th port, to switch off all the other ports and calculate the n-th current.

The desired radiation conditions are achieved using an antenna with a pencil beam radiation pattern in order to radiate only one sub-area of the target. The other cells are not directly illuminated with this incident field (see Fig. 3). It is worth highlighting that the required radiation conditions can be easily achieved using an internal option of the code CST that does not require the implementation of the geometry of the antenna. The simulation of this scenario gives us the induced current density on the whole surface of the target: in particular, the field and the current values in each central point of each sub-area are sampled from the CST results to evaluate the matrix elements in Equation (3). Since for each run of the computer, which corresponds to a specific radiation condition, we are able to calculate all the elements of a column of the admittance matrix, the program must be iterated N times for each polarization. It is important to outline that generally the commercial code provides the total electric field into a penetrable target or the total tangential magnetic field for highly conducting materials, and therefore further assumptions are necessary to obtain the currents.

The procedure to calculate the current induced on the surface

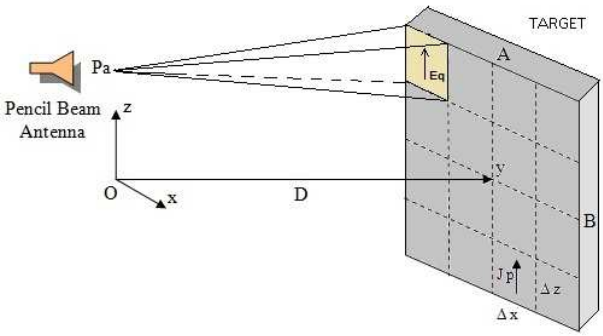

Figure 3. Incident electric field over the q-th subsurface of the human thorax model. A pencil beam antenna was used for the matrix Y evaluation.

of the plane depends on the value of the dielectric parameters of the plate. When the plate is made with a high conductive element, the current is simply equal to the tangential component of the magnetic field on the surface. When the plate is made with a lossy dielectric, the current is obtained from the tangential electric field component using the following relation:

$$\vec{J}_p = [\sigma + j\omega(\varepsilon - \varepsilon_0)] \left(\frac{\delta}{1+j}\right) \vec{E}_p \tag{4}$$

where σ is the conductivity of the material, ε its permittivity, and δ the penetration depth of the electromagnetic field.

The far field pattern of the ideal antenna, used to radiate selectively each sub-area, is shown in Fig. 4 for the Phi = 90° and Theta = 90° plane. It is symmetric on both E-plane and H-plane and positioned 1 m far from the subsurface aiming to its center.

This ideal radiation pattern is imported analytically in the CST project, and it is used to radiate the target.

The choice of the subsurface dimensions is a tradeoff between the accuracy of the model results, the possibility to model the respiratory activity and the computational time.

Once the Y matrix is known it is possible to calculate the current density on the target and the reflected field from the knowledge of the characteristics of whatever antenna radiating the incident field, using Equations (1) and (2).

In the particular case of the breath monitoring the useful

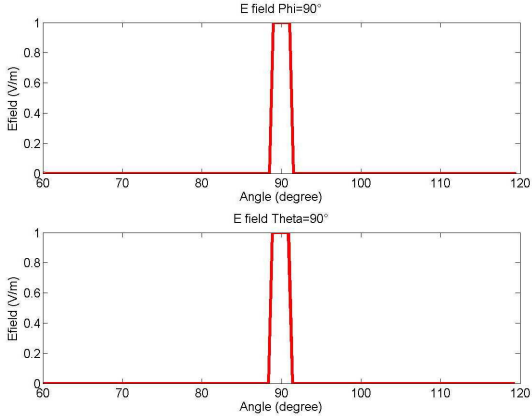

Figure 4. Ideal antenna far field pattern used for the matrix Y evaluation.

parameter that has to be derived is the scattering parameter S_{11} at the input of the antenna, because from the time history of its amplitude or phase it is possible to obtain the breathing frequency. This parameter depends on the type of antenna used in the system. In the case of an aperture antenna, as the one used in our results, from the scattered field the s_{11} parameter at the input of the antenna is calculated as:

$$S_{11} = \Gamma_a + \Gamma_{sc} l_{eff} \sqrt{\frac{2\eta\left(1 - |\Gamma_a|^2\right)}{Z_0 ab}} \frac{Z_0}{Z_a + Z_0} \tag{5}$$

where Γ_a is the reflection coefficient of the antenna in free space, Γ_{sc} the ratio between the radiated field and the reflected field, and l_{eff} the effective length of the antenna. Z_0 and Z_a are respectively the impedance of the cable feeding the antenna and the input impedance of the antenna, and a and b are the dimension of the aperture. The detailed procedure to achieve Equation (5) is reported in appendix.

3. EXPERIMENTAL VALIDATION

In Fig. 1(a) vector network analyzer (VNA) generates the continuous signal at the chosen frequency. It performs a continuous low power measurement of the reflection coefficient and its phase variation is used to recover the respiration activity. A rectangular metallic panel with dimensions of 0.4 m by 0.4 m and a dielectric box made with plexiglass (2 mm thick) filled with a lossy dielectric are chosen for the model validation tests. The inner dimension of the dielectric box are 40 cm × 40 cm × 2.5 cm.

The antenna used for transmitting and receiving the electromagnetic energy is a broadband, double ridged horn antenna, having a measured gain of 8.6 dBi at 2 GHz and 8.9 dBi at 3 GHz. In the numerical model, an equivalent aperture over a ground plane, having the same half power beam width (HPBW) as the double ridge antenna, is used in order to model the far field of the antenna, analytically calculated. Its main beam is aligned to the center of the target, which was placed at a distance varying in the range from 0.5 m to 2.5 m. In order to mimic the thorax movement during breathing activity, the target is displaced periodically around its initial position, in this way the phase and the amplitude of the s_{11} parameter are modulated, and their values are used to validate the method, comparing theoretical and experimental data. The measurements were carried out inside an anechoic environment in order to reduce the unwanted reflection from reflecting objects inside the laboratory.

The discretization adopted for the target was chosen studying the convergence of the method.

In Fig. 5 is reported the maximum theoretical phase variations of the reflected signal due to a 1 cm displacement of the metallic plate placed at different distances from the antenna. The plate is discretized with $N \times N$ elements with N that varies from 4 to 10.

From Fig. 5 it can be noted that the method converges with few discretization elements.

In the proposed method the accuracy is achieved using two different discretization steps. The first is used when implementing the CST procedure and it is based on the standard numerical approach, typically $\lambda/20$. The second, shown in Fig. 5, determines the dimension of the Y matrix, and it depends on the uniformity of the current on the target surface.

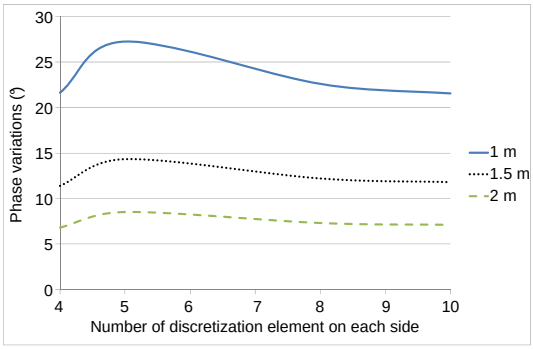

Figure 5. Convergence test: the discretization of the plate was varied from 4 to 10 elements per each side of the plate.

3.1. Metallic Plate

A first scenario considers the metallic panel positioned perpendicularly to the antenna main beam direction. The phase variation of the S_{11} parameter due to the plate displacement was measured and calculated at different distance from the antenna. In Fig. 6 an example of the phase modulation when the target displaces around its central position is reported. In this example the target is placed at 2.05 m from the antenna, and the frequency of the signal is 3 GHz. We can observe that the model is able to simulate with a satisfactory agreement the measured data.

The maximum phase variation (the peak to peak value in Fig. 6) during the periodically movement, for each distance is recorded and

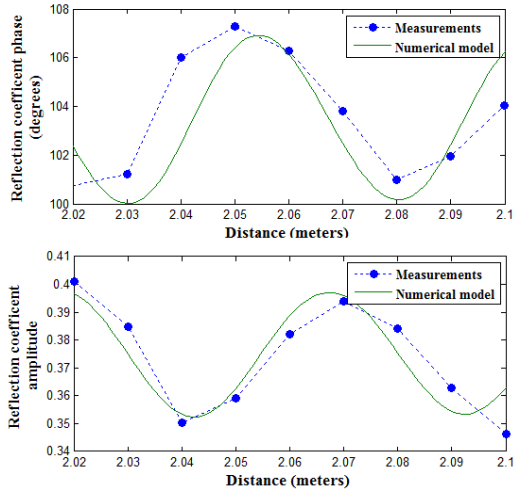

Figure 6. Example of model output results, compared to measurements, at $f = 3\,\text{GHz}$ and $d = 2.05\,\text{m}$.

the results are shown in Fig. 7. The distances varied from 50 cm to 250 cm and measurements were done every 50 cm. Also in this case the comparison between simulations and measurements is quite satisfactory; the lower accuracy in the short distance range is due to the far field assumption of the model that fails in this operating context. A displacement of about 10 cm is obviously too long to be representative of a breathing activity, which normally consists in a variation of the chest position of about 1 or 2 cm. However, the results highlight two main aspects: the first is the capability of the method to sense effectively also displacements of one or two centimeters, as shown in Fig. 6; the second aspect is the sensitivity that depends on the sample position, i.e., it is low in correspondence of a maximum or a minimum of the oscillation, whereas it is high between them. This result suggests that the use of a single frequency should be avoided, in order to eliminate critical situations.

A second scenario considers the metallic panel slightly rotated around its initial position by 10 degrees and 20 degrees. The same positions along the y-axis are considered, as in the previous scenario. The admittance matrix used in this second scenario is exactly the same used for the first one. The maximal phase variations in these cases are shown respectively in Fig. 8 and Fig. 9 for the operating frequency of 2 GHz (a) and 3 GHz (b).

The good level of agreement between the measurement results and

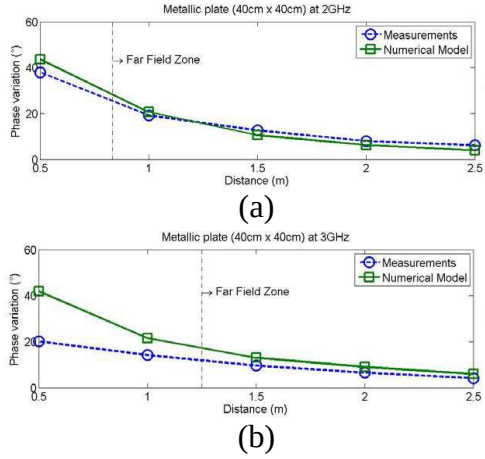

Figure 7. Maximum phase variation for different target distances: Models and measurement results for the operating frequency of (a) 2 GHz and (b) 3 GHz.

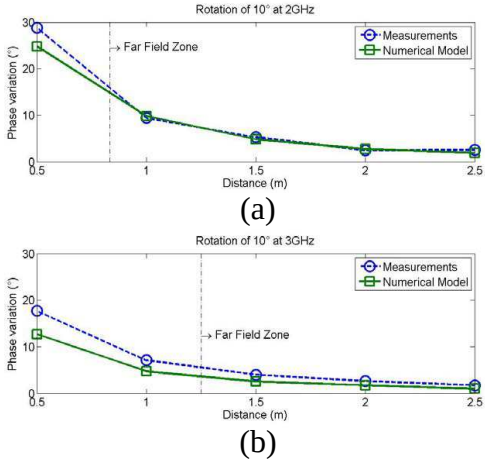

Figure 8. Model and measurement results for the operating frequency of (a) 2 GHz and (b) 3 GHz. The metallic plane was rotated to 10°.

the electromagnetic model results shows that the admittance matrix calculated with our method provides a general approach that depends only on the geometry of the target and not on its position, and moreover can be used also for impinging fields different from those used to determine the matrix terms.

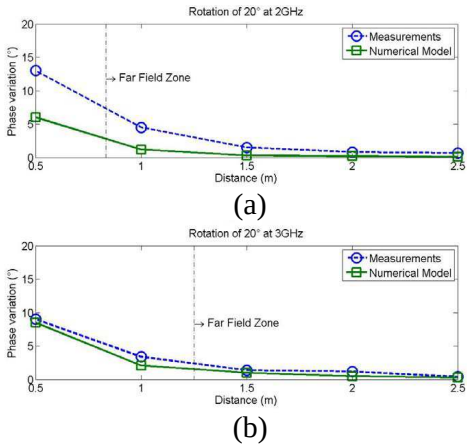

Figure 9. Model and measurement results for the operating frequency of (a) 2 GHz and (b) 3 GHz. The metallic plane was rotated to 20°.

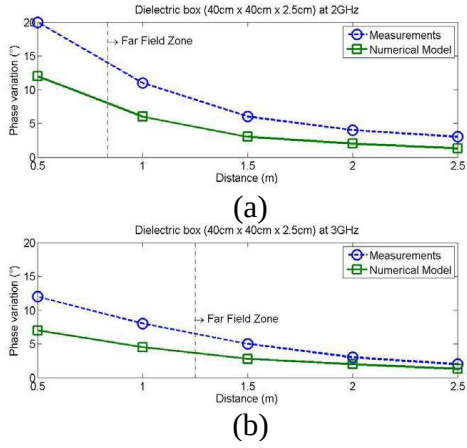

Figure 10. Model and measurement results for the operating frequency of (a) 2 GHz and (b) 3 GHz. As a scatterer a dielectric rectangular box of 40 cm × 40 cm × 2.5 cm was used.

3.2. Dielectric Box

The dielectric box is filled with salty water having conductibility $\sigma = 3.1\,\mathrm{S/m}$ and relative permittivity $\varepsilon_r = 74$. The penetration depth is 1.498 cm at 2 GHz and 1.484 cm at 3 GHz, the operating frequencies considered in the test. The values of the penetration depth allow to consider satisfactory the assumption of a 2-D geometry of the body.

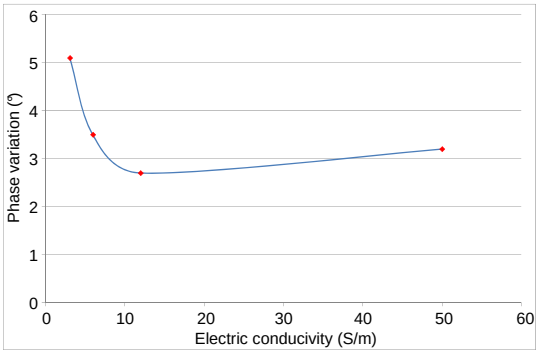

Figure 11. Maximum phase variation for the reflected signal from a dielectric object with different conductivity values.

As for the metallic plate the target was placed at different distances from the antenna, and at each position it was periodically displaced by mimicking the respiration act. The maximum phase variation of the S_{11} parameter, for each distance considered, is shown in Fig. 10.

From the figure it can be noted that the application of the model to the dielectric object provides less accurate results in comparison with results achieved for the metallic surface. These discrepancies suggested us to investigate the effects of the uncertainty of dielectric parameters on result accuracy. Fig. 11 reports the maximum phase variation when a dielectric target is considered. The operating distance is 1 m and the material conductivity ranges from 3 up to 50 S/m, whereas the relative permittivity is 74.

It is interesting to note that the human muscle has a conductivity of 3 S/m at 3 GHz, therefore the system sensitivity is the highest for chosen parameter.

We can observe that in the range of low conductivity values, result strongly depends on the material characteristics and therefore this can explain the differences between theoretical and experimental results shown in Fig. 10, where the conductivity was estimated with empirical formulas and not directly measured.

4. CONCLUSIONS

A simple model for the characterization of electromagnetic scattering is presented. Even if results concern a specific application, i.e., monitoring of the breathing activity of an exposed subject, the method is general and applicable to other types of scattering problems. The basic idea is to obtain the admittance matrix of the target using a

numerical tool. The main advantage of this model is that it permits parametric analysis of the problem as an analytical model, without the necessity of repeating each time the calculation of the admittance matrix because it is an intrinsic characteristic of the target. The comparison between the simulations and measurements shows good agreement. Work is in progress to extend the model to more complex and realistic geometries.

APPENDIX A.

The calculation of the S_{11} parameter considers both the reflection due to the antenna itself and the reflection due to the target placed in front of the antenna.

When the antenna is placed in an open space the reflected voltage at the input terminals of the antenna depends only on the antenna itself, and, for a matched generator, is:

$$V^- = \frac{V_g}{2} e^{j\beta L} \frac{Z_i - Z_0}{Z_i + Z_0} \tag{A1}$$

where V_g is the open circuit voltage of the generator, $Z_i = Z_0 \frac{e^{j\beta L} + \Gamma_{ant} e^{-j\beta L}}{e^{j\beta L} - \Gamma_{ant} e^{-j\beta L}}$ is the input impedance of the antenna seen at the generator port, Z_0 is the characteristic impedance of the line, and L is the length of the feeding line. For the voltage received by the antenna and due to the field reflected by a target placed in front of it, the equivalent circuit of the receiving antenna shown in Fig. A1 is considered.

The voltage V_{rx}, that represents the Thevenin (open circuit) generator of the circuit, is the voltage received by the antenna. Z_{ant} is the input impedance of the antenna, and Z_0 is the generator impedance. By definition

$$V_{rx} = \vec{E}_{sc} \cdot \vec{l}_{eff} = E_z^{sc} l_{eff} = \Gamma_{sc} E_0^{tr} l_{eff} \tag{A2}$$

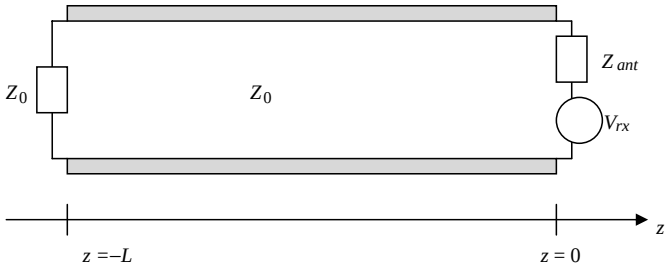

Figure A1. Equivalent circuit of the antenna in receiving mode.

where l_{eff} is the vector effective length of the antenna [16], $\Gamma_{sc} = \frac{E_z^{sc}}{E_0^{tr}} = \frac{\sum_{n=1}^{N} E_{nz}}{E_0^{tr}}$, E_0^{tr} and E_z^{sc} are, respectively, the electric field radiated by the antenna and the electric field scattered by the target, calculated at the antenna. Equation (A2) is particularized for the antenna considered in our example that is linearly polarized along z. Considering the classical transmission line theory, the voltage injected along the line in backward direction by the V_{rx} generator is,

$$V^- = V_{rx} \frac{Z_0}{Z_{ant} + Z_0} = \Gamma_{sc} E_0^{tr} l_{eff} \frac{Z_0}{Z_{ant} + Z_0} \tag{A3}$$

The total voltage wave travelling in the negative z-direction is given by Equations (A3) and (A1).

From the definition of S_{11} parameter we obtain:

$$S_{11} = \frac{V_{TOT}^-}{V^+} = \frac{\frac{V_g}{2} e^{j\beta L} \frac{Z_i - Z_0}{Z_i + Z_0} + \Gamma_{sc} E_0^{tr} l_{eff} \frac{Z_0}{Z_{ant} + Z_0}}{\frac{V_g}{2} e^{-j\beta L}} \tag{A4}$$

In our case the antenna is an equivalent aperture ($a \times b$) with a uniform field distribution, and so E_0^{tr} can be calculated as a function of V_g from the radiated power:

$$W_{rad} = \frac{V_g^2}{8Z_0} \left(1 - |\Gamma_{\text{ant}}|^2\right) = \frac{1}{2\eta} \int_{Aperture} \left|E_{ap}^{tr}(x,y)\right|^2 dxdy = \frac{1}{2\eta} \left|E_0^{tr}\right|^2 ab \tag{A5}$$

Replacing Equation (A5) in Equation (A4), Equation (5) is obtained.

REFERENCES

1. Harrington, R. F., *Field Computation by Moment Methods,* Oxford University Press, USA, 1993
2. Draine, B. T. and P. J. Flatau, "Discrete-dipole approximation for scattering calculations," *Journal of the Optical Society of America A: Optics and Image Science, and Vision*, Vol. 11, No. 4, 1491–1499, 1994
3. Coccioli, R., T. Itoh, G. Pelosil, and P. P. Silvester, "Finite-elements methods in microwaves: A selected bibliography," *IEEE Antennas Propagation Magazine*, Vol. 38, No. 6, 34–48, 1996.
4. Taflove, A. and S. C. Hagness, *Computational Electrodynamics*, 160, Artech house, Boston, London, 2000.
5. Yang, P. and K. N. Liou, "Finite difference time domain method for light scattering by non spherical and inhomogeneous particles," *Light Scattering by Non spherical Particles: Theory, Measurements, and Applications*, M. I. Mishchenko, J. W. Hovenier, and L. D. Travis (eds.), Academic Press, New York, 2000.

6. Hadi, M. F. and M. Piket-May, "A modified FDTD (2, 4) scheme for modelling electrically large structures with high-phase accuracy," *IEEE Trans. Antennas Propagation*, Vol. 45, No. 2, 254–264, 1997.
7. Manry, C. W., S. L. Broschat, Jr., and J. B. Schneider, "Higher order FDTD methods for large problems," *ACES Journal*, Vol. 10, 17–29, 1995.
8. Sarkar, T. and S. Rao, "The application of the conjugate gradient method for the solution of electromagnetic scattering from arbitrarily oriented wire antennas," *IEEE Trans. Antennas Propagation*, Vol. 32, No. 4, 398–403, 1984.
9. Michalski, K. A. and J. R. Mosig, "Multilayered media Green's functions in integral equation formulations," *IEEE Trans. Antennas Propagation*, Vol. 45, No. 3, 508–519, 1997.
10. Cerri, G., R. De Leo, and V. Mariani Primiani, "A rigorous model for radiated emission prediction in PCB circuits," *IEEE Trans. on Electromagnetic Compatibility*, Vol. 35, No. 1, 102–109, 1993.
11. Kolundzija, B. M., "Electromagnetic modeling of composite metallic and dielectric structures," *IEEE Transactions on Microwave Theory and Techniques*, Vol. 47, No. 7, 1021–1032, 1999.
12. Cerri, G., P. Russo, A. Schiavoni, G. Tribellini, and P. Bielli, "MoM-FDTD hybrid technique for analysing scattering problems," *Electronic Letters*, Vol. 34, No. 5, 438–440, 1998.
13. Abd-Alhameed, R. A., P. S. Excell, M. A. Mangoud, and J. A. Vaul, "Computation of radiated and scattered field using separate frequency domain moment-method regions and frequency domain MoM-FDTD hybrid methods," *Proceedings of the 1999 IEE National Conference on Antennas and Propagation*, 53–56, York, UK, Mar. 1999.
14. Scalise, L., V. Mariani Primiani, P. Russo, A. De Leo, D. Shahu, and G. Cerri, "Wireless sensing for the respiratory activity of human beings: Measurements and wide-band numerical analysis," *International Journal of Antennas and Propagation*, Vol. 2013, Article No. 396459, ISSN: 16875869, Doi: 10.1155/2013/396459.
15. Microwave Studio, CST-Computer Simulation Technology, Bad Nuheimer Str. 19, 64289 Darmstadt, Germany, 2010.
16. Balanis, C. A., *Antenna Theory: Analysis and Design*, John Wiley & Sons, Publishers, Inc., New York, 2005.